

Article

# Low-Cost Electrodeposition of Size-Tunable Single-Crystal ZnO Nanorods

Elias Sakellis <sup>1,2</sup> , Antonis Markopoulos <sup>1</sup>, Christos Tzouvelekis <sup>1</sup>, Manolis Chatzigeorgiou <sup>1</sup>, Anastasios Travlos <sup>1</sup> and Nikos Boukos <sup>1,\*</sup> 

- <sup>1</sup> National Centre for Scientific Research “Demokritos”, Institute of Nanoscience and Nanotechnology, 15310 Agia Paraskevi Attikis, Greece; e.sakellis@inn.demokritos.gr (E.S.); antmarko@hotmail.com (A.M.); christzouvelekis@gmail.com (C.T.); e.chatzigeorgiou@inn.demokritos.gr (M.C.); a.travlos@inn.demokritos.gr (A.T.)
- <sup>2</sup> Section of Solid State Physics, Physics Department, University of Athens, Panepistimiopolis, Zografos, 15684 Athens, Greece
- \* Correspondence: n.boukos@inn.demokritos.gr

**Abstract:** In this paper we report a low cost, simple, electrochemical method for large-area growth of single crystal ZnO nanorods. The method utilizes a metallic zinc foil as the source of the necessary zinc ions for ZnO growth on indium-doped tin oxide (ITO) glass slides. The method is thoroughly discussed and investigated varying all the parameters involved. The resulting ZnO nanorods are highly oriented along c-axis and densely packed, while their length and diameter can be tuned by varying the growth parameters. Two different types of seed layers on the ITO glass slides are tested. A seed layer made by spin coating of ZnO nanoparticles results in a twofold increase of the ZnO nanorod surface density as compared with a ZnO thin film seed layer by physical vapor deposition. Additionally, the effect of oxygen supply during electrodeposition was investigated as a crucial regulatory parameter not only for the geometrical and topological characteristics of the ZnO nano-arrays but for their physical properties as well.

**Keywords:** ZnO; nanorods; electrochemical method; oxygen; nanoparticles; electrodeposition



**Citation:** Sakellis, E.; Markopoulos, A.; Tzouvelekis, C.; Chatzigeorgiou, M.; Travlos, A.; Boukos, N. Low-Cost Electrodeposition of Size-Tunable Single-Crystal ZnO Nanorods. *Fibers* **2021**, *9*, 38. <https://doi.org/10.3390/fib9060038>

Academic Editor: Vijay Kumar Thakur

Received: 16 April 2021  
Accepted: 1 June 2021  
Published: 7 June 2021

**Publisher's Note:** MDPI stays neutral with regard to jurisdictional claims in published maps and institutional affiliations.



**Copyright:** © 2021 by the authors. Licensee MDPI, Basel, Switzerland. This article is an open access article distributed under the terms and conditions of the Creative Commons Attribution (CC BY) license (<https://creativecommons.org/licenses/by/4.0/>).

## 1. Introduction

Among the transparent oxides, ZnO stands of great importance. It is a wide and direct bandgap ( $E_g = 3.23\text{--}3.42$  eV), II–VI semiconductor, with relatively large exciton binding energy (about 60 meV) at room temperature and high electron mobility [1]. The aforementioned -among others- properties are the reason of a plethora of applications concerning ZnO. Solar cells, photocatalytic cells, sensors and optoelectronics are only few of these fields. [2–6] There are several techniques used for zinc oxide growth with prime desiderata the high quality and the low cost [7]. Electrodeposition is a promising candidate method which attempts to fulfil the previously cited needs. The main advantage of electrodeposition in general is its simplicity, while, varying at will the electrochemical parameters affects the structural as well as the physical properties of the resultant ZnO layers [8–12]. To the best of our knowledge, the established electrodeposition methods utilize zinc salts as the source of the required zinc ions for the growth of ZnO nanostructures, as well as other salts for supporting electrolytes [9,13–16]. The use of chloride or nitrate salts may result in intentional [14,15] or unintentional [16] incorporation of anions impurities such as  $\text{Cl}^-$  in the ZnO structure affecting ZnO growth and electronic properties.

In this work a very simple, fast, low temperature, low equipment cost and time expense, electrodeposition method for growing ZnO nanorods is presented. Its simplicity originates from the use of only two electrodes as compared to the commonly reported three electrode electrodeposition methods, while it does not require salts for supporting electrolyte or any pH adjustment [9,13–16]. The combination of a zinc metallic foil used

as counter-electrode and aqueous formamide solution employed as electrolyte provides the necessary zinc for the growth of ZnO, whereas no additional metal cations or chloride/nitrate anions are present that may lead to the incorporation of undesirable impurities in the ZnO crystal [14–16]. The proposed electrodeposition method is about ten times faster than previously reported chemical bath ones utilizing formamide solutions [17], being comparable with the established three electrode methods employing zinc salts [9]. The resulting ZnO rods are homogeneously grown, highly oriented and densely packed while their diameter is controllable. The method has been tested on indium-doped tin oxide (ITO) coated glass substrates utilizing two different seed layers: (i) a thin ZnO film prepared by Electron-Beam Physical Vapor Deposition (EBPVD), (procedure A) and (ii) a thin film made by spin-coating of ZnO nanoparticles (procedure B). Furthermore, the morphology and properties of the ZnO nanorods was investigated changing the oxygen concentration in the electrodeposition bath solution, while using a spin-coating seed layer (procedure C).

## 2. Materials and Methods

### 2.1. Materials and Cleaning Procedure

Indium-doped tin oxide ITO sputtered glasses (5–15  $\Omega/\square$  at room temperature), purchased from Delta Technologies Ltd., Loveland, CO, USA, were used as substrates after thorough cleaning. This step was crucial for the subsequent ZnO layers adherence to the substrate and homogeneity. At first, the glasses were sonicated within a 2% *v/v* solution of alkaline liquid concentrate (Hellmanex III) in de-ionized water (DI water) for 30 min and after that meticulously rinsed with DI water. Next, the glasses were ultrasonically cleaned in acetone and IPA, for 10 min each, rinsing with DI water in-between. Finally, the substrates were cleaned with a solution of 3% HCl acid and 1% HNO<sub>3</sub> acid, rinsed with DI water and dried under nitrogen gas flow.

Zinc foils (99.9% Sigma-Aldrich, St. Louis, MO, USA) were used after been carefully cleaned with acetone and absolute ethanol.

Finally, analytical grade formamide (Sigma Aldrich, St. Louis, MO, USA) was used to prepare aqueous solutions with DI water.

### 2.2. Preparation of ZnO Seed Layers

#### 2.2.1. EBPVD

ZnO pellets, initially made by cold pressing of ZnO powder (99.9995% Alfa Aesar, Ward Hill, MA, USA), were used as target material in a high vacuum chamber ( $10^{-4}$  Pa base pressure), equipped with 2 electron guns. ZnO thin films of 50 nm thickness were deposited by e-beam evaporation on the ITO/glass substrates at room temperature. The deposition rate varied from 1.2 nm/s to 1.5 nm/s, as monitored by a calibrated quartz crystal microbalance. Next, the seeded substrates were annealed at 300 °C for 15 min in air.

#### 2.2.2. ZnO Nanoparticles (NPs)

ZnO nanoparticles were synthesized according to Haase et al. [18] and with the combination of other, similar to the previous [19], methods. In particular, 2.95 gr zinc acetate dehydrated, and 1.48 gr KOH (0.5 M) were dissolved in 125 mL and 65 mL of methanol, respectively. The first solution was heated to 60 °C under vigorous stirring and then the potassium hydroxide solution was gradually added within 15 min. The resulting solution was vigorously stirred for 2 h at 60 °C. Next, the solution was left to sit without heating or stirring for another two hours. Subsequently, the supernatant liquid was removed from the precipitated nanoparticles, 50 mL of methanol was added, and the solution was centrifuged. Finally, 5 mL of chloroform and 25 mL of methanol was added to the residuum nanoparticles. The final solution of the nanoparticles was used to spin-coat the ITO glasses with a thin film of ZnO nanoparticles. Lastly, the substrates were annealed for 15 min at 300 °C in air to improve cohesion of the ZnO thin film on the ITO glasses.

### 2.3. Electrochemical Growth of ZnO Nanorods (NRs)

The electrolyte was a formamide aqueous solution of various concentrations (Table 1) containing Zn complexes, which was created by immersing a cleaned zinc foil in an aqueous solution formamide for 18 h. The ZnO seeded substrate was used as the working electrode while a cleaned zinc foil was used as the counter electrode. The 1.25 cm × 3.50 cm electrodes were positioned at a distance of 2.5 cm, facing each other. A constant voltage of 0.3 V, with respect to the Zn foil, was applied to the working electrode by a Metrohm Autolab PGSTAT204 potentiostat. The electrolyte temperature was kept constant at 65 °C ± 1 °C in a bath. The solution was stirred, and the current was monitored throughout the electrodeposition. Growth times could be varied from a few minutes to few hours, depending on the desirable dimensions of the ZnO formed. After growth, the samples were rinsed in distilled water and ethanol, and finally dried by nitrogen gas flow.

**Table 1.** Experimental data for different formamide concentrations for each of the three procedures A, B and C: formamide concentration C, length  $L_{rod}$ , diameter  $D_{rod}$  and the aspect ratio  $L_{rod}/D_{rod}$  of ZnO nanorods, the transferred charge during electrochemical growth, the density of ZnO nanorods, the optical energy gap  $E_{g,opt}$  calculated from UV-vis measurements and the wavelength of the maximum intensity from PL spectra.

Procedure A							
Growth Method: Electrodeposition Seeding Layer: ZnO Film (EBPVD) O <sub>2</sub> Supply: No							
Formamide C (% vol)	$L_{rod}$ (nm)	$D_{rod}$ (nm)	$L_{rod}/D_{rod}$	Charge (C)	Density $\rho$ (rods/ $\mu\text{m}^2$ )	$E_{g,opt}$ (eV)	PL Peak (nm)
0.05%	480	70	6.9	1.206	31	3.31	396
0.1%	640	75	8.5	1.378	38	3.34	380
0.5%	750	85	8.8	2.374	23	3.31	376
1%	900	95	9.5	5.452	21	3.33	381
Procedure B							
Growth Method: Electrodeposition Seeding Layer: Chem. Synthesized ZnO NPs (Spin Coating) O <sub>2</sub> Supply: No							
Formamide C (% vol)	$L_{rod}$ (nm)	$D_{rod}$ (nm)	$L_{rod}/D_{rod}$	Charge (C)	Density $\rho$ (rods/ $\mu\text{m}^2$ )	$E_{g,opt}$ (eV)	PL Peak (nm)
0.05%	300	40	7.5	1.246	60	3.31	380
0.1%	490	50	9.8	1.527	64	3.31	380
0.5%	690	65	10.6	3.226	45	3.33	380
1%	810	75	10.8	4.099	43	3.35	376
Procedure C							
Growth Method: Electrodeposition Seeding Layer: Chem. Synthesized ZnO NPs (Spin Coating) O <sub>2</sub> Supply: Yes							
Formamide C (% vol)	$L_{rod}$ (nm)	$D_{rod}$ (nm)	$L_{rod}/D_{red}$	Charge (C)	Density $\rho$ (rods/ $\mu\text{m}^2$ )	$E_{g,opt}$ (eV)	PL Peak (nm)
0.05%	590	80	7.4	2.217	30	3.27	381
0.1%	630	75	8.4	2.883	32	3.26	380
0.5%	1040	100	10.4	6.223	30	3.30	381
1%	1500	125	12.0	9.787	25	3.31	380

### 2.4. Characterization

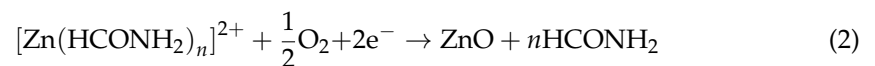
The morphology of the resulting nanostructures was determined by scanning electron microscopy (SEM) using an FEI Inspect microscope, operating at a voltage of 25 kV. Transmission Electron Microscopy (TEM) was undertaken utilizing an FEI CM20 microscope operating at 200 kV. TEM specimens of the grown nanostructures were prepared by scraping off the substrates and placing them on carbon support copper TEM grids. In order to examine the ZnO nanoparticles 5  $\mu\text{L}$  of the final solution were drop-casted on the same type of TEM grids followed by evaporation at ambient conditions. Powder X-ray diffraction (XRD) spectra, with  $2\theta$  range 25–80°, were acquired with a SIEMENS D500 Bragg Brentano diffractometer, using Cu K $\alpha$  radiation ( $\lambda = 0.15418$  nm), step-size 0.03° and measuring time 2 s/step. Photoluminescence (PL) measurements were carried out using

a Horiba Jobin-Yvon iHR320 Spectrometer with a He–Cd laser (325 nm) as the excitation source. UV-Visible (UV-Vis) absorption measurements were obtained with a Shimadzu, UV2100 UV-VIS split-beam spectrophotometer in a wavelength range of 250 nm to 900 nm, employing an ITO glass-slide as reference.

### 3. Results and Discussion

Several experiments have been carried out in order to investigate thoroughly the role of each one of the parameters involved in the growth process. As mentioned in the introduction, three procedures were carried out that aim not only to present and investigate this growth method but also to examine the role of the seed layer on the growth (comparing procedures A and B), as well as to control the dimensions and photoluminescence of the grown ZnO nanorods (comparing procedures B and C). It should be mentioned that all subsequent results concern a typical two hour electrodeposition growth.

The ZnO growth mechanism could be described by the following steps: Zinc-formamide complexes are formed in the vicinity of the Zn foil, counter-electrode and are subsequently transferred to the substrate, working electrode, under the applied electrical field. There, Zn reacts with oxygen and finally ZnO is formed. The two reactions which take place during growth are:



at the Zn foil and at the substrate region, respectively [17,20,21].

Scanning electron microscopy images (Figure 1), transmission electron microscopy images (Figure 2), X-ray diffraction spectra (Figure 3), photoluminescence measurements (Figure 4) and UV-Visible absorption measurements (Figure 5), provide information for the topology, crystallinity, the composition and the electronic structure of ZnO.

From the SEM images (Figure 1), regardless of which procedure was followed, it becomes apparent that the substrate is uniformly covered with hexagonal ZnO rods preferentially oriented perpendicular to the substrate. It should be noted that the synthesized nanorod arrays display lateral homogeneity across the whole substrate area, i.e., about  $33 \times 10 \text{ mm}^2$ , making this growth method promising to be upscaled to larger areas. X-ray diffraction patterns (Figure 4) verifies that that no other phase except for wurtzite ZnO (JPDS 36-1451) was grown during this electrochemical method. Furthermore, depicted are ITO peaks (JPDS 6-416) originating from the substrate. The texture coefficient TC for the ZnO (002) peak is calculated [22] from the following equation:

$$\text{TC}_{(002)} = \frac{I_{(002)}/I_{(002)}^0}{1/N \sum I_{(hkl)}/I_{(hkl)}^0} \quad (3)$$

where  $N$  is the number of the diffraction peaks,  $I_{(hkl)}$  and  $I_{(hkl)}^0$  are the measured and reported in the JCPDS 36-1451 intensities, respectively. The  $\text{TC}_{(002)}$  values are 3.5, 3.8 and 4.8 for procedures A, B and C, respectively. These high values indicate that the nanorods are textured and well-aligned with the c-axis perpendicular to the substrate [22,23], in agreement with the SEM results. Moreover, the degree of texturing increases from Procedure A to Procedure C. It has been reported that the growth of the more initially inclined rods is impeded, whereas it is favored for the more vertically oriented ones for geometry reasons [22,23]. As can be seen in Table 1, the surface density of ZnO nanorods grown by Procedure B is twice that by Procedure A, leaving less available space for the growth of inclined nanorods, thus increasing texturing coefficient. On the other hand, nanorods grown by Procedure C have the highest length and aspect ratio, leading to the maximum value of TC.

Dimensional information deduced from the SEM images is quantified (Table 1) and plotted (Figure 6). The general trend is that the length, diameter and aspect ratio increase

when formamide concentration is increased in each procedure, since there are more Zn atoms available, as transferred charge confirms (see Table 1).

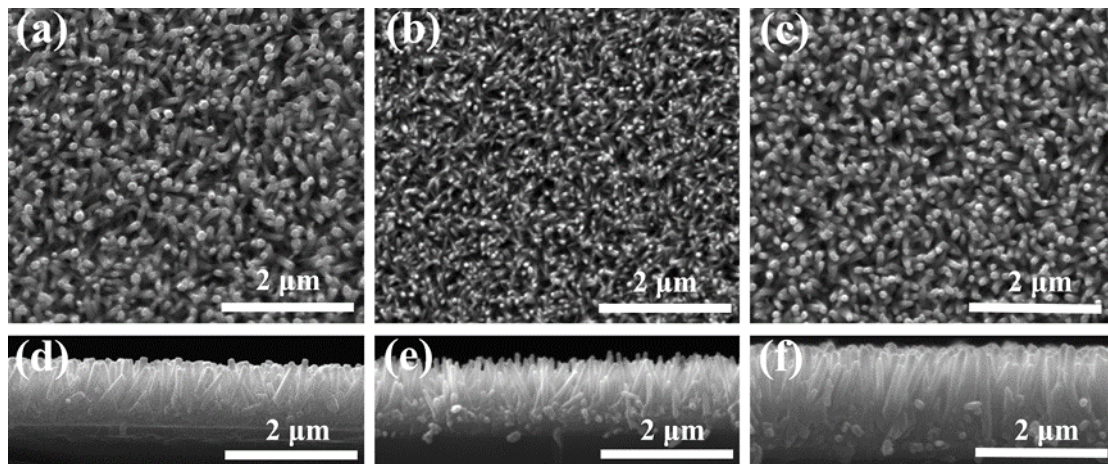


**Figure 1.** SEM images—plane view and cross section- of the ZnO nanorods grown in 0.5% formamide for each of the three procedures A (a,d), B (b,e) and C (c,f) respectively.

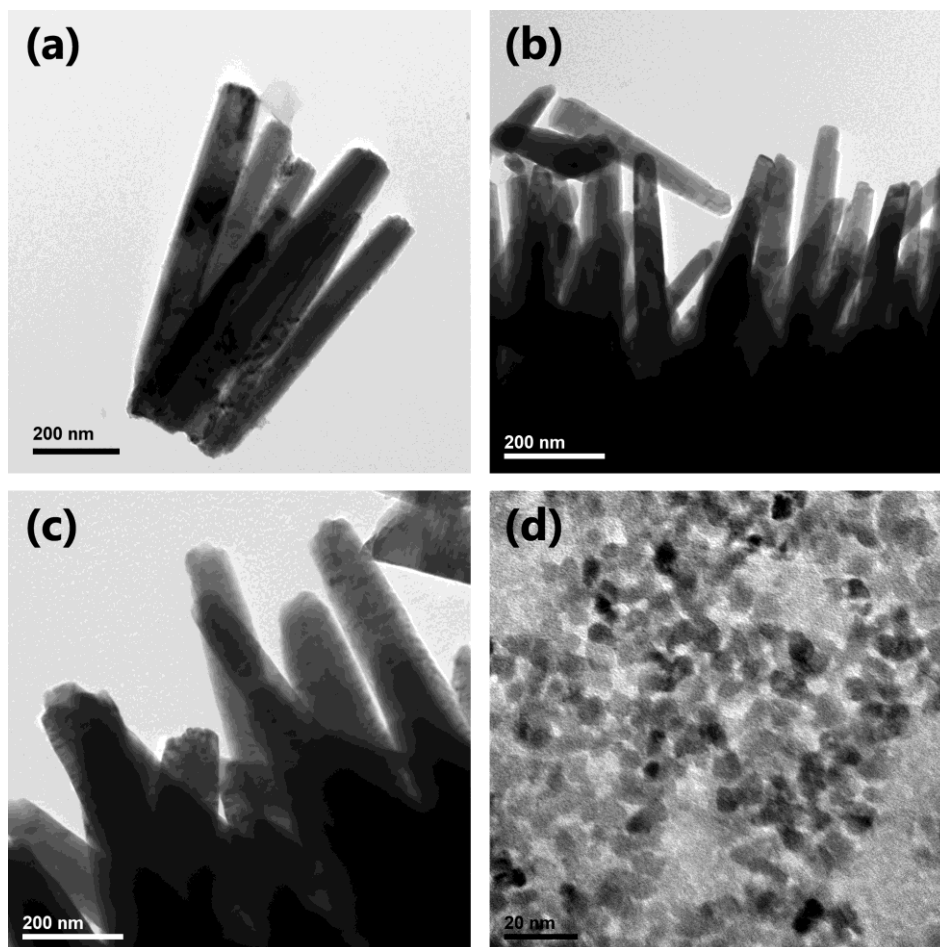


**Figure 2.** Bright field TEM images of the ZnO nanorods grown in 0.5% formamide for each of the three procedures A (a), B (b) and C (c) and of ZnO nanoparticles used for the spin-coating seed layer (d).

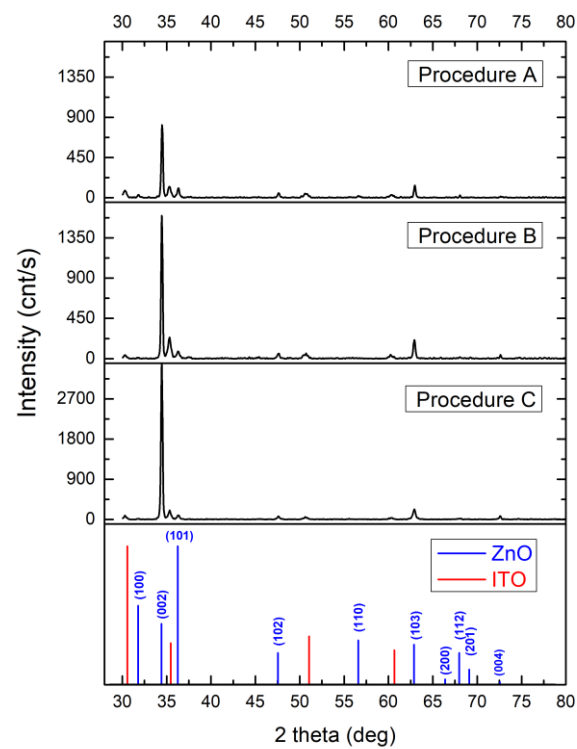


**Figure 3.** X-ray diffraction spectrum of ZnO nanorods grown in 0.5% formamide for each of the three procedures A, B and C.

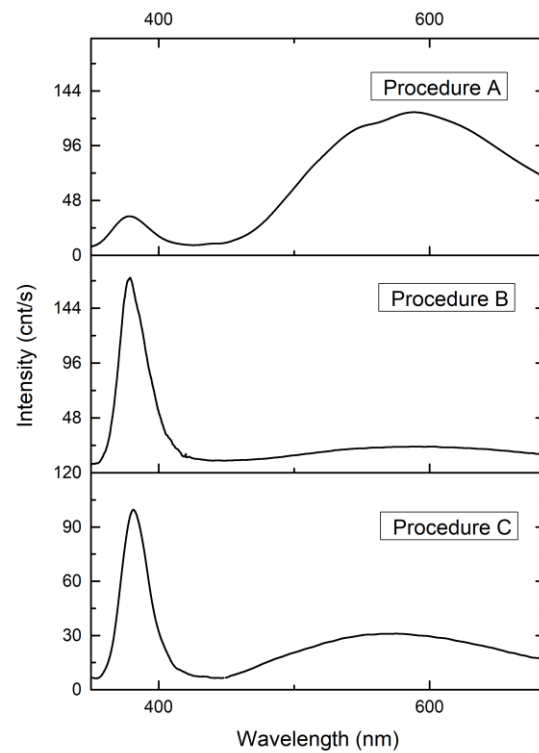


**Figure 4.** Room temperature photoluminescence spectra of the ZnO nanorods grown in 0.5% formamide for each of the three procedures A, B and C.

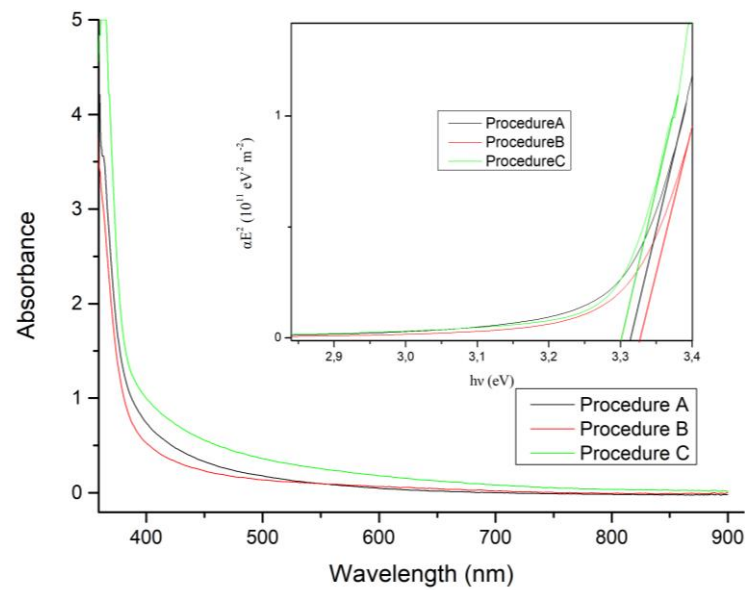


**Figure 5.** UV-vis transmittance spectra of the ZnO nanorods grown in 0.5% formamide for each of the three procedures A, B and C. Inset:  $(\alpha E)^2$  versus  $E$ —where  $E$  is the photon energy and  $\alpha$  is the absorption coefficient.

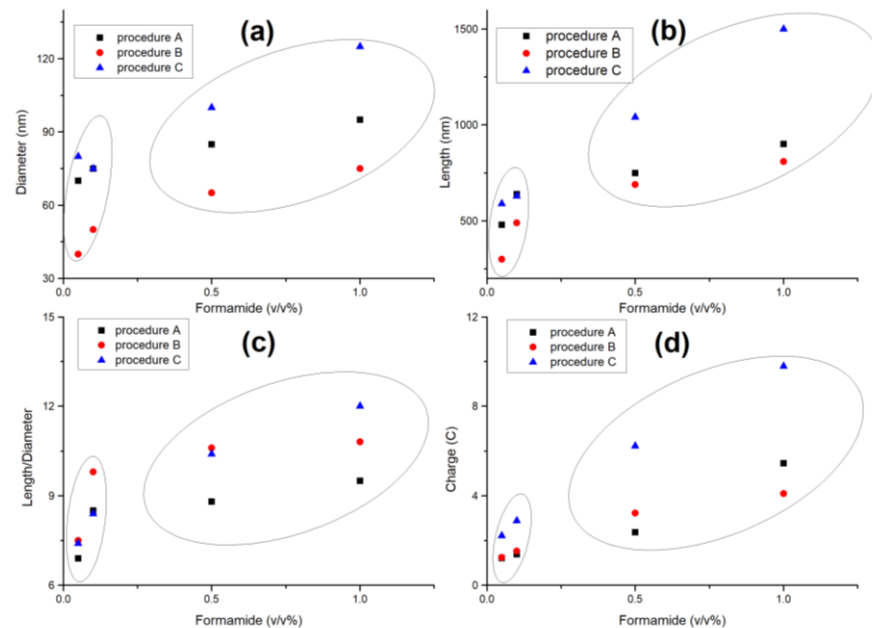


**Figure 6.** Diameter (a), length (b), and aspect ratio (c) of the ZnO nanorods as well as the charge (d) transferred during electrodeposition for each of the three procedures A, B and C.

On the other hand, the density of ZnO rods appears to increase at first and then as formamide concentration is further increased, the density of rods decreases in each procedure. Raising formamide concentration leads to an increase of Zn complexes that results to an increment of “starting points” on the seed layer and therefore, to a raise in rod density. As formamide concentration is further increased, the density of “starting points” on the seed layer exceeds some value above which nanorods are growing very close to each other resulting to their coalescence and consequent reduction of their density.

It is well known that there is an anisotropic growth along  $c$ -axis, since the growth rate in  $\langle 001 \rangle$  direction is larger than that of  $\langle 101 \rangle$  and  $\langle 100 \rangle$  [24–26]. Thus, different growth rates are expected in the two directions, the one parallel  $r_p$  and the other vertical  $r_v$  to the

growth axis. The ratio of these rates determines the aspect ratio of each rod, i.e.,  $r_p/r_v \sim l/d$ . Moreover, if the ratio  $r_p/r_v(t)$  varies as a function of time the diameter  $d$  of the rod will change along its length  $l$ . Since the diameter of each nanorod diminishes along its growth direction (Figures 1 and 3), it can be concluded that  $r_p/r_v(t)$  is an ascending function of time. This could be attributed to a gradual change of the electrochemical environment—for example the local electric field—in the vicinity of the corresponding surfaces of the growing nanorods resulting in a pyramidal shape of the nanorods (Figure 3).

The role of the seeding layer on the electrochemical growth of ZnO nanorods can be determined comparing the nanorods grown utilizing procedures A and B. It is evident from the data presented in Table 1, that a major difference is the surface density of the nanorods grown by the two procedures, i.e., a twofold increase of the nanorods density is achieved when a spin-coating seed layer (procedure B) is used instead of an EBPVD thin film layer (procedure A). This difference can be explained as follows: ZnO nanocrystals on the seeding layer act as preferred nucleation centers for the growth of ZnO nanorods. The mean crystallite size of the seed layer in procedure B is 3–8 nm corresponding to the mean ZnO nanoparticle size shown in the TEM micrograph (Figure 2d). On the other hand, the mean crystallite size of the EBPVD thin film layer used in procedure A is expected to be in the range of its thickness [27], that is roughly 20–40 nm. Consequently, the smaller crystallite size in the spin coating seed layer leads to a higher nuclei density for the initial ZnO precipitation, resulting in an increased surface density of the ZnO nanorods grown by procedure B.

UV-Visible (UV-Vis) absorption measurements (Figure 6) allowed for an estimation of the optical energy gap  $E_{g,opt}$  (Table 1), by plotting (Figure 6 inset) the  $(\alpha E)^2$  versus  $E$ —where  $E$  is the photon energy and  $\alpha$  is the absorption coefficient—and extrapolating the (increasing) linear part of the curve. The optical energy gap was evaluated according to Equation (4) that describes the energy dependence  $E$  of the absorption coefficient  $\alpha$  [28] in the case of direct band gap semiconductors:

$$\alpha \propto \sqrt{h\nu - E_{g,opt}} / (h\nu) \quad (4)$$

The optical energy gaps calculated from UV-Vis measurements for each one of the procedures and for various formamide concentrations are tabulated in Table 1.

The PL spectra of zinc oxide nanorods for each procedure are presented at Figure 5. All the PL spectra exhibit a peak at 380 nm which is attributed to the recombination of free excitons [29]. Moreover, a broad peak including green (around 520 nm) and yellow-orange (around 600 nm) is observed [30]. This broad band is attributed to intrinsic defects of ZnO [10,31,32]. More specifically, this band is due to several kinds of defects: the green between 490 nm and 530 nm, is frequently attributed to oxygen vacancies, zinc vacancies, zinc interstitials, oxygen antisites and transitions between the latter two [33–43]. The yellow luminescence (around 590 nm) is usually attributed to interstitial oxygen [43,44]. Thus, supplying additional oxygen during growth (procedure C) results in an enhancement of the aforementioned part of the spectrum as compared to that corresponding to procedure B during which no excess oxygen is supplied.

The present growth method is versatile and has several advantages over previously proposed growth methods. It is reported that ZnO nanorods can be grown utilizing a Zn foil and a seeded substrate immersed in a formamide solution at about 65 °C for several hours (24 h [17], 60 h [20], 20 h [24]). With the present method, the procedure is greatly accelerated, while the good quality of the crystal is preserved. The electric field facilitates the constant flow of zinc-formamide complexes resulting in an enhanced ZnO growth rate at least an order of magnitude higher than the ones previously reported [9,17,24]. Furthermore, whereas most of the reported methods [9,13–16] use salts in the growth solution, that act either as zinc source or support conductivity of the electrolyte, the present method employs only a metallic zinc foil. Hence there are no impurities that could be incorporated in the ZnO crystal during growth. Changing formamide concentration alters the availability of

Zn complexes. Whilst the ratio of zinc to oxygen concentration is lower than one, raising the formamide concentration up to ~0.1% results to an approximately linear increment of the growth rate. As the formamide concentration is further increased, the ratio of zinc to oxygen concentration tends to one and the growth rate decreases with a saturation trend (Figure 2, Procedures A and B). Additional oxygen supply lowers the aforementioned ratio of concentrations, and the linear growth rate is extended to higher zinc concentrations (Figure 2, Procedure C). Thus, control of oxygen inflow and zinc complexes supply, can be used to tailor the ZnO nanorods dimensions as well as to incorporate excess oxygen or zinc atoms in the crystal structure, altering the type of the intrinsic defects and resulting to different physical properties of the ZnO nanorods.

#### 4. Conclusions

Single crystalline ZnO nanorods of controllable length, diameter and density were grown by a novel, simple and electrodeposition method on seeded ITO glass substrates. The method utilizes a counter electrode of metallic zinc foil to provide the necessary zinc ions, while no reference electrode, no salts (employed as zinc source or supporting electrolyte) and no pH adjustment are required. The absence of cations other than those of Zn ensures that no impurities are incorporated in the ZnO structure during growth. The ZnO nanorod arrays are vertically well-aligned and textured with the *c*-axis perpendicular to the substrate, while they are homogeneously distributed over the whole substrate area of about 3 cm<sup>2</sup>, making this growth method promising to be upscaled to larger areas. The increase of concentration of the organic solvent results in an enhancement of the growth rate and aspect ratio of the ZnO nanorods due to the increased supply of Zn ions, while oxygen bubbling during growth, apart from enhancing growth rate, also increases the yellow luminescence that is attributed to the formation of oxygen interstitials in the ZnO lattice. Finally, the utilization of a spin-coated seeding layer, comprised of ZnO nanoparticles, doubles the ZnO nanorod surface density compared to that of an EBPVD seeding layer, due to the smaller crystallite size of the former.

**Author Contributions:** Conceptualization, E.S. and N.B.; methodology, A.M., A.T. and E.S.; investigation, formal analysis, A.M., C.T. and M.C.; writing—original draft preparation, E.S. and N.B.; writing—review, A.T. All authors have read and agreed to the published version of the manuscript.

**Funding:** This research was partly funded by the project “National Infrastructure in Nanotechnology, Advanced Materials and Micro-/Nanoelectronics” (MIS 5002772) which is implemented under the Action “Reinforcement of the Research and Innovation Infrastructure”, funded by the Operational Programme “Competitiveness, Entrepreneurship and Innovation” (NSRF 2014–2020) and co-financed by Greece and the European Union (European Regional Development Fund).

**Conflicts of Interest:** The authors declare no conflict of interest.

#### References

1. Özgür, Ü.; Alivov, Y.I.; Liu, C.; Teke, A.; Reshchikov, M.A.; Doğan, S.; Avrutin, V.; Cho, S.J.; Morkoç, H. A comprehensive review of ZnO materials and devices. *J. Appl. Phys.* **2005**, *98*, 041301. [[CrossRef](#)]
2. Willander, M.; Nur, O.; Zhao, Q.X.; Yang, L.L.; Lorenz, M.; Cao, B.Q.; Pérez, J.Z.; Czekalla, C.; Zimmermann, G.; Grundmann, M.; et al. Zinc oxide nanorod based photonic devices: Recent progress in growth, light emitting diodes and lasers. *Nanotechnology* **2009**, *20*, 332001. [[CrossRef](#)] [[PubMed](#)]
3. Bhati, V.S.; Hojamberdiev, M.; Kumar, M. Enhanced sensing performance of ZnO nanostructures-based gas sensors: A review. *Energy Rep.* **2020**, *6*, 46–62. [[CrossRef](#)]
4. Theerthagiri, J.; Salla, S.; Senthil, R.; Nithyadharseni, P.; Madankumar, A.; Arunachalam, P.; Maiyalagan, T.; Kim, H.-S. A review on ZnO nanostructured materials: Energy, environmental and biological applications. *Nanotechnology* **2019**, *30*, 392001. [[CrossRef](#)]
5. Serrà, A.; Gómez, E.; Philippe, L. Bioinspired ZnO-Based Solar Photocatalysts for the Efficient Decontamination of Persistent Organic Pollutants and Hexavalent Chromium in Wastewater. *Catalysts* **2019**, *9*, 974. [[CrossRef](#)]
6. Qadir, A.M.; Erdoğan, I.Y. Structural properties and enhanced photoelectrochemical performance of ZnO films decorated with Cu<sub>2</sub>O nanocubes. *Int. J. Hydrog. Energy* **2019**, *44*, 18694–18702. [[CrossRef](#)]
7. Borysiewicz, M.A. ZnO as a Functional Material: A Review. *Crystals* **2019**, *9*, 505. [[CrossRef](#)]

8. Kumar, R.; Kumar, G.; Al-Dossary, O.; Umar, A. ZnO nanostructured thin films: Depositions, properties and applications—A review. *Mater. Express* **2015**, *5*, 3–23. [[CrossRef](#)]
9. Kumar, M.; Sasikumar, C. Electrodeposition of Nanostructured ZnO Thin Film: A Review. *Am. J. Mater. Sci. Eng.* **2014**, *2*, 18–23. [[CrossRef](#)]
10. Kołodziejczak-Radzimska, A.; Jesionowski, T. Zinc Oxide—From Synthesis to Application: A Review. *Materials* **2014**, *7*, 2833–2881. [[CrossRef](#)]
11. Singh, G.; Singh, P.S. Synthesis of zinc oxide by sol-gel method and to study its structural properties. *AIP* **2020**, *2220*, 020184.
12. Aldalbahi, A.; Alterary, S.; Almoghim, R.A.A.; Awad, M.A.; Aldosari, N.S.; Alghannam, S.F.; Alabdian, A.N.; Alharbi, S.; Alateeq, B.A.M.; Mohsen, A.; et al. Greener Synthesis of Zinc Oxide Nanoparticles: Characterization and Multifaceted Applications. *Molecules* **2020**, *25*, 4198. [[CrossRef](#)] [[PubMed](#)]
13. Skompska, M.; Zarebska, K. Electrodeposition of ZnO Nanorod Arrays on Transparent Conducting Substrates—A Review. *Electrochim. Acta* **2014**, *127*, 467–488. [[CrossRef](#)]
14. Xu, L.; Guo, Y.; Liao, Q.; Zhang, J.; Xu, D. Morphological Control of ZnO Nanostructures by Electrodeposition. *J. Phys. Chem. B* **2005**, *109*, 13519–13522. [[CrossRef](#)]
15. Alev, O.; Sarica, N.; Ozdemir, O.; Arslan, L.Ç.; Büyükköse, S.; Oztürk, Z.Z. Cu-doped ZnO nanorods based QCM sensor for hazardous gases. *J. Alloys Compd.* **2020**, *826*, 154177. [[CrossRef](#)]
16. Lupan, O.; Pauporte, T.; Chow, L.; Viana, B.; Pelle, F.; Ono, L.K.; Cuenya, B.R.; Heinrich, H. Effects of annealing on properties of ZnO thin films prepared by electrochemical deposition in chloride medium. *Appl. Surf. Sci.* **2010**, *256*, 1895–1907. [[CrossRef](#)]
17. Boukos, N.; Chandrinou, C.; Giannakopoulos, K.; Pistolis, G.; Travlos, A. Growth of ZnO nanorods by a simple chemical method. *Appl. Phys. A* **2007**, *88*, 35–39. [[CrossRef](#)]
18. Haase, M.; Weller, H.; Henglein, A. Photochemistry and radiation chemistry of colloidal semiconductors. 23. Electron storage on zinc oxide particles and size quantization. *J. Phys. Chem.* **1988**, *92*, 482–487. [[CrossRef](#)]
19. Seow, Z.L.S.; Wong, A.S.W.; Thavasi, V.; Jose, R.; Ramakrishna, S.; Ho, G.W. Controlled synthesis and application of ZnO nanoparticles, nanorods and nanospheres in dye-sensitized solar cells. *Nanotechnology* **2008**, *20*, 045604. [[CrossRef](#)] [[PubMed](#)]
20. Zhang, Z.; Yu, H.; Shao, X.; Han, M. Near-Room-Temperature Production of Diameter-Tunable ZnO Nanorod Arrays through Natural Oxidation of Zinc Metal. *Chem. A Eur. J.* **2005**, *11*, 3149–3154. [[CrossRef](#)] [[PubMed](#)]
21. Sakellis, I.; Giamini, S.; Moschos, I.; Chandrinou, C.; Travlos, A.; Kim, C.-Y.; Lee, J.-H.; Kim, J.-G.; Boukos, N. A novel method for the growth of Cu<sub>2</sub>O/ZnO heterojunctions. *Energy Proc.* **2014**, *60*, 37–42. [[CrossRef](#)]
22. Lupan, O.; Guérina, V.M.; Tiginyanub, I.M.; Ursakib, V.V.; Chowc, L.; Heinrichc, H.; Pauporté, T. Well-aligned arrays of vertically oriented ZnO nanowires electrodeposited on ITO-coated glass and their integration in dye sensitized solar cells. *J. Photochem. Photobiol. A* **2010**, *211*, 65–73. [[CrossRef](#)]
23. Pauporte, T.; Bataille, G.; Joulaud, L.; Vermersch, F.J. Well-aligned ZnO nanowire arrays prepared by seed-layer-free electrodeposition and their Cassie–Wenzel transition after hydrophobization. *J. Phys. Chem. C* **2010**, *114*, 194–202. [[CrossRef](#)]
24. Zhang, Z.; Yu, H.; Wang, Y.; Han, M.-Y. Aggregation-driven growth of well-oriented ZnO nanorod arrays. *Nanotechnology* **2006**, *17*, 2994–2997. [[CrossRef](#)]
25. Li, W.J.; Shi, E.W.; Zhong, W.Z.; Yin, Z.W. Growth mechanism and growth habit of oxide crystals. *J. Cryst. Growth* **1999**, *203*, 186–203. [[CrossRef](#)]
26. Ahsanulhaq, Q.; Umar, A.; Hahn, Y.B. Growth of aligned ZnO nanorods and nanopencils on ZnO/Si in aqueous solution: Growth mechanism and structural and optical properties. *Nanotechnology* **2007**, *18*, 115603. [[CrossRef](#)]
27. Mbam, S.O.; Nwonu, S.E.; Orelaja, O.A.; Nwigwe, U.S.; Gou, X.-F. Thin-film coating; historical evolution, conventional deposition technologies, stress-state micro/nano-level measurement/models and prospects projection: A critical review. *Mater. Res. Express* **2019**, *6*, 122001. [[CrossRef](#)]
28. Kumar, J.; Srivastava, A.K. Band gap narrowing in zinc oxide-based semiconductor thin films. *J. Appl. Phys.* **2014**, *115*, 134904. [[CrossRef](#)]
29. Meyer, B.K.; Alves, H.; Hofmann, D.M.; Kriegseis, W.; Forster, D.; Bertram, F.; Christen, J.; Hoffmann, A.; Straßburg, M.; Dworzak, M.; et al. Bound exciton and donor–acceptor pair recombinations in ZnO. *Phys. Status Solidi* **2004**, *241*, 231–260. [[CrossRef](#)]
30. Rodnyi, P.A.; Khodyuk, I.V. Optical and luminescence properties of zinc oxide (Review). *Opt. Spectrosc.* **2011**, *111*, 776–785. [[CrossRef](#)]
31. Chris, A.J.; Van De Walle, G. Fundamentals of zinc oxide as a semiconductor. *J. Cryst. Growth* **2006**, *72*, 126501.
32. Sakellis, I. Determining the activation volumes in ZnO. *J. Appl. Phys.* **2012**, *112*, 13504. [[CrossRef](#)]
33. Kohan, A.F.; Ceder, G.; Morgan, D.; Van De Walle, C.G. First-principles study of native point defects in ZnO. *Phys. Rev. B* **2009**, *61*, 15019. [[CrossRef](#)]
34. Guo, B.; Qiu, Z.R.; Wong, K.S. Intensity dependence and transient dynamics of donor–acceptor pair recombination in ZnO thin films grown on (001) silicon. *Appl. Phys. Lett.* **2003**, *82*, 2290. [[CrossRef](#)]
35. Liu, W.; Gua, S.L.; Ye, J.D.; Zhu, S.M.; Liu, S.M.; Zhou, X.; Zhang, R.; Shi, Y.; Zheng, Y.D. Blue-yellow ZnO homostructural light-emitting diode realized by metalorganic chemical vapor deposition technique. *Appl. Phys. Lett.* **2006**, *88*, 092101. [[CrossRef](#)]
36. Leiter, F.H.; Alves, H.R.; Hofstaetter, A.; Hofmann, D.M.; Meyer, B.K. The Oxygen Vacancy as the Origin of a Green Emission in Undoped ZnO. *Phys. Status Solidi* **2001**, *226*, R4–R5. [[CrossRef](#)]
37. Leiter, F.H.; Alves, H.; Pfisterer, D.; Romanov, N.G.; Hofmann, D.M.; Meyer, B.K. Identification of oxygen and zinc vacancy optical signals in ZnO. *Physica B* **2003**, *201*, 340.
38. Liu, M.; Kitai, A.; Mascher, P. Point defects and luminescence centres in zinc oxide and zinc oxide doped with manganese. *J. Lumin.* **1992**, *54*, 35–42. [[CrossRef](#)]

39. Reynolds, D.C.; Look, D.C.; Jogai, B.; Hoelscher, J.E.; Sherriff, R.E.; Harris, M.T.; Callahan, M.J. Time-resolved photoluminescence lifetime measurements of the  $\Gamma_5$  and  $\Gamma_6$  free excitons in ZnO. *J. Appl. Phys.* **2000**, *88*, 2152. [[CrossRef](#)]
40. Dingle, R. Luminescent Transitions Associated With Divalent Copper Impurities and the Green Emission from Semiconducting Zinc Oxide. *Phys. Rev. Lett.* **1969**, *23*, 579. [[CrossRef](#)]
41. Studenikin, S.A.; Golego, N.; Cocivera, M. Fabrication of green and orange photoluminescent, undoped ZnO films using spray pyrolysis. *J. Appl. Phys.* **1998**, *84*, 2287. [[CrossRef](#)]
42. Alivov, Y.I.; Chukichev, M.V.; Nikitenko, V.A. Green luminescence band of zinc oxide films copper-doped by thermal diffusion. *Semiconductors* **2004**, *38*, 31–35. [[CrossRef](#)]
43. Chandrinou, C.; Boukos, N.; Stogios, C.; Travlos, A. PL study of oxygen defect formation in ZnO nanorods. *Microelectron. J.* **2009**, *40*, 296–298. [[CrossRef](#)]
44. Travlos, A.; Boukos, N.; Chandrinou, C.; Kwack, H.-S.; Dang, L.S. Zinc and oxygen vacancies in ZnO nanorods. *J. Appl. Phys.* **2009**, *106*, 104307. [[CrossRef](#)]